

Article

Nitrate Removal and Dynamics of Microbial Community of A Hydrogen-Based Membrane Biofilm Reactor at Diverse Nitrate Loadings and Distances from Hydrogen Supply End

Minmin Jiang ^{1,2,†}, Yuanyuan Zhang ^{1,†}, Yuhang Yuan ², Yuchao Chen ², Hua Lin ², Junjian Zheng ^{1,*}, Haixiang Li ^{2,*} and Xuehong Zhang ^{1,2}

¹ College of Life and Environmental Science, Guilin University of Electronic Technology, 1 Jinji Road, Guilin 541004, China; jiangminmin1015@163.com (M.J.); zhangyuanyuan0226@hotmail.com (Y.Z.); zhangxuehong@x263.net (X.Z.)

² College of Environmental Science and Engineering, Guilin University of Technology, 319 Yanshan Street, Guilin 541006, China; joweyh@outlook.com (Y.Y.); 1020180208@glut.edu.cn (Y.C.); linhua@glut.edu.cn (H.L.)

* Correspondence: zhengjunjianglut@163.com (J.Z.); 2011042@glut.edu.cn (H.L.)

† These authors contributed to the work equally and should be regarded as co-first authors.

Received: 4 September 2020; Accepted: 13 November 2020; Published: 15 November 2020



Abstract: The back-diffusion of inactive gases severely inhibits the hydrogen (H₂) delivery rate of the close-end operated hydrogen-based membrane biofilm reactor (H₂-based MBfR). Nevertheless, less is known about the response of microbial communities in H₂-based MBfR to the impact of the gases' back-diffusion. In this research, the denitrification performance and microbial dynamics were studied in a H₂-based MBfR operated at close-end mode with a fixed H₂ pressure of 0.04 MPa and fed with nitrate (NO₃⁻) containing influent. Results of single-factor and microsensors measurement experiments indicate that the H₂ availability was the decisive factor that limits NO₃⁻ removal at the influent NO₃⁻ concentration of 30 mg N/L. High-throughput sequencing results revealed that (1) the increase of NO₃⁻ loading from 10 to 20–30 mg N/L resulted in the shift of dominant functional bacteria from *Dechloromonas* to *Hydrogenophaga* in the biofilm; (2) excessive NO₃⁻ loading led to the declined relative abundance of *Hydrogenophaga* and basic metabolic pathways as well as counts of most denitrifying enzyme genes; and (3) in most cases, the decreased quantity of N metabolism-related functional bacteria and genes with increasing distance from the H₂ supply end corroborates that the microbial community structure in H₂-based MBfR was significantly impacted by the gases' back-diffusion.

Keywords: back-diffusion; biofilm; denitrification; microbial community; nitrate loading

1. Introduction

Nitrate (NO₃⁻) contamination of surface and groundwater has become a significant challenge due to the uncontrolled discharge of wastewater and the intensive use of fertilizers [1,2]. Given the organic-deficient nature of surface and groundwater (in which, the content of dissolved organic matter is commonly below 18 mg/L) [3,4], the autotrophic denitrification technique is therefore a more reasonable option than its heterotrophic counterpart, despite the higher biodegradation kinetics rate of the latter. As an emerging autotrophic denitrification approach, H₂-based membrane biofilm reactor (H₂-based MBfR), has gained widespread popularity in recent years for the purification of NO₃⁻-contaminated surface and groundwater, mainly attributed to the unique advantages, namely, allowing efficient and cost-effective NO₃⁻ elimination with minimal bio-sludge yield and without

need for external carbon source [5–7]. In H_2 -based MBfR, H_2 gas, the exogenous electron donor, driven by the H_2 -concentration gradient across the walls of the hollow-fiber membranes (HFMs), diffuses passively from the intramembrane to the HFMs-attached biofilm. In the biofilm, H_2 is oxidized by the denitrifying bacteria (DNB) to reduce the NO_3^- that diffuses from the bulk liquid [8]. Given the abundant presence of inorganic carbon (mainly bicarbonate) in most surface and groundwater [9–11], the denitrification performance of the H_2 -based MBfR system is commonly largely dependent on the availability of H_2 and NO_3^- within the counter-diffusional biofilm.

The gas-based MBfR is usually operated with either open-end or close-end HFMs. In the case of open-end operation, due to the markedly higher gas velocity of advective transport in the intramembrane than the diffusive transfer across the walls of HFMs, the intramembrane gas was uniformly distributed with an elevated concentration level, which enables the high microbial activity in the biofilm along the HFMs [12]. Nonetheless, in addition to the massive loss of gas, the open-end operation is inapplicable to H_2 -based MBfR as it creates an explosive atmosphere. Alternatively, the H_2 -based MBfR is extensively equipped with close-end HFMs, on account of electron donor (i.e., H_2) saving and operational safety [13–15]. Unfortunately, close-end HFMs always suffer from the back-diffusion of inactive gases such as nitrogenous and water vapor gases, especially the N_2 from bulk liquid and hydrogenotrophic denitrification process, which may severely reduce the overall HFM efficiency in terms of H_2 delivery [8,12,16]. According to a previous model-predicted result, the gas transfer rate of HFMs operated at the open-end mode was obviously greater than that of the close-end operation, leading to an approximately 116% increase in the contaminant removal flux of the system [12].

As displayed in Figure 1, in principle, as a result of the continuous H_2 consumption by the biofilm along the HFMs, accompanied by the back-diffusion of inactive gases (mainly N_2) from the biofilm and bulk liquid into the intramembrane as well as the flow of gases toward the distal end of HFMs, the partial pressure of H_2 and N_2 gradually increases and decreases with the increase in distance from the H_2 supply end, respectively; the diffusion of N_2 from the intramembrane into the biofilm is due to its concentration at the end of the HFMs [5]. Until now, to the best of our knowledge, only one single research exists that covers the effects of gas back-diffusion on the gas profiles of biofilm, the gas transfer rate of membrane, and the pollutant removal efficiency of the gas-based membrane biofilm reactor system [12]. No study has been published to give insights into the impacts of gas back-diffusion on the dynamics of a microbial community in H_2 -based MBfR. Research is needed to address this knowledge gap. The objectives of this study are as follows: (1) to evaluate how the denitrification performance of H_2 -based MBfR responds to influent NO_3^- concentration variation, and (2) to reveal the evolution of the microbial community structure in the biofilm with changing NO_3^- loadings and distances from the H_2 supply end.

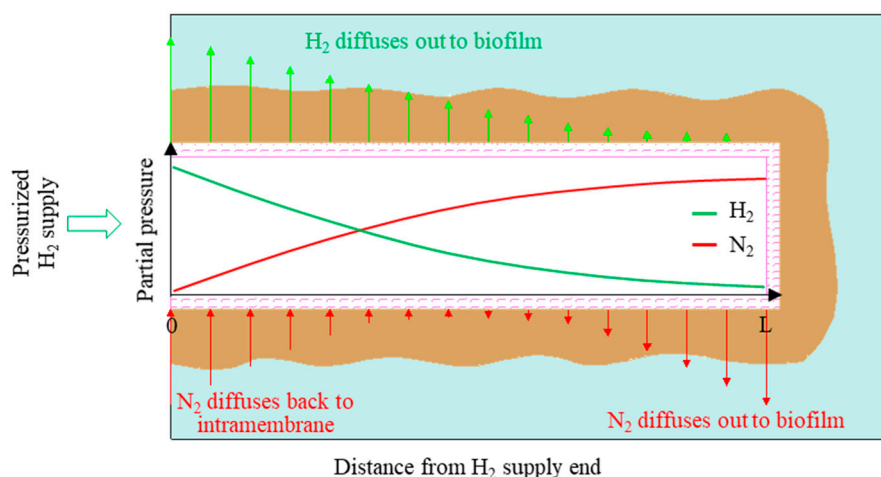


Figure 1. Pressurized H_2 supply and N_2 back diffusion in a close-end hollow-fiber membrane (HFM).

2. Materials and Methods

2.1. Reactor Configuration

A schematic of the lab-scale H₂-based MBfR used in this study is shown in Figure 2. The reactor contained 20 polyvinyl chloride made HFMs (effective length = 450 mm, inner diameter = 1.0 mm, outer diameter = 1.5 mm, pore size = 0.01 μm, membrane surface area = 0.042 m²) assembled in a vertical plexiglass cylindrical shell (inner diameter = 45 mm, height = 500 mm, effective volume = 0.6 L). An ultrapure H₂ tank was connected to the lower end of the HFM module for pressurized H₂ supplementation. The upper end of the module was sealed using waterproof epoxy glue. A gas regulator was linked to the H₂ tank for H₂ supplying pressure adjustment. Synthetic medium (see Section 2.2 for details) was pumped from the bottom of the reactor via a peristaltic pump (BT101L-DG-1, Lead Fluid, Baoding, China). To guarantee the complete mixing of bulk liquid, a recirculation pump (BT101L-YZ15/25, Lead Fluid, Baoding, China) was operated at a high flowrate of 100 mL/min. Effluent was collected from the outlet at the top of the reactor.

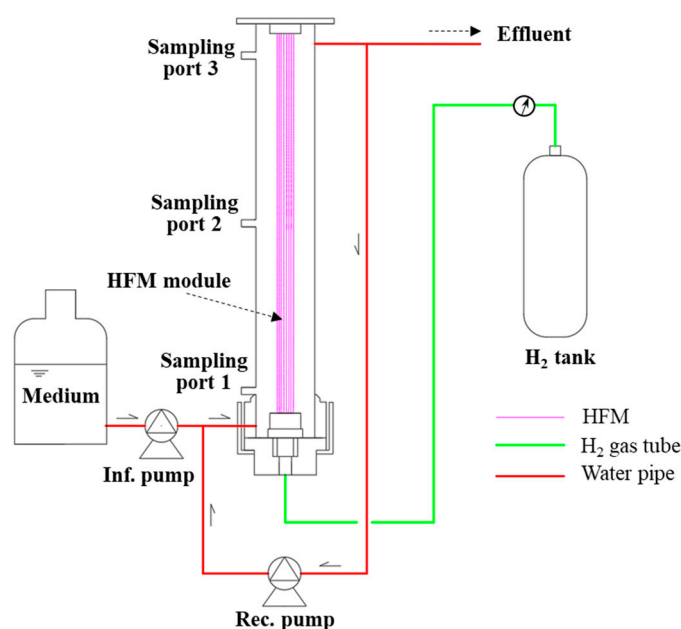


Figure 2. Schematic of the H₂-based membrane biofilm reactor (MBfR) setup.

2.2. Synthetic Influent

The synthetic influent was prepared using tap water amended with NaNO₃, NaHCO₃, and mineral trace elements. NO₃[−] was added according to the demand, and 252 mg/L NaHCO₃ was added as the sole carbon source to maintain the autotrophic bacteria growth [13]. The composition of mineral trace elements was identical to our previous study (in μg/L) [17]: 1000, CaCl₂·2H₂O; 1000, FeSO₄·7H₂O; 13, ZnSO₄·7H₂O; 4, MnCl₂·4H₂O; 38, H₃BO₃; 25, CoCl₂·6H₂O; 1, CuCl₂·2H₂O; 1, NiCl₂·6H₂O; 4, Na₂MoO₄·2H₂O; and 4, Na₂SeO₃. The bulk liquid pH was adjusted to around 7.5 with phosphate buffer (216 mg/L Na₂HPO₄·12H₂O + 236 mg/L KH₂PO₄) to eradicate the impact of pH drop on the denitrification performance. The synthetic medium was purged with pure N₂ for 30 min to maintain the anaerobic condition of the influent prior to entering the reactor [18].

2.3. Experimental Operation

The inoculated biomass was obtained from a long-term operated denitrifying H₂-based MBfR in our lab [19]. A H₂ pressure of 0.04 MPa was used throughout the whole experiment period, which is a quintessential empirical parameter extensively implemented in preceding H₂-based MBfRs [9,13,20].

The start-up processes of the reactor were as follows: a relatively low influent NO_3^- concentration of 10 mg N/L was initially used to facilitate the start-up of the reactor, and the influent flowrate was set at 1 mL/min, resulting in a hydraulic retention time (HRT) of 10 h; once the complete removal of NO_3^- was achieved, the influent flowrate was increased to 2 mL/min, corresponding to an HRT of 5 h. Following experiments, in which the influent NO_3^- concentration was sequentially maintained at 10, 20, and 30 mg N/L in phases I, II and III, respectively, were carried out to investigate the effects of NO_3^- availability on the denitrification performance of the system and the dynamics of microbial communities in biofilm. In each phase, 40 days operation was performed to enable the system performance and microbial community structure to reach stabilization. Specifically, a NO_3^- influent concentration of 10–30 mg N/L was adopted since this range is close to the typical NO_3^- concentration in real contaminated groundwater [21–23], and is the representative concentration range extensively investigated in H_2 -based MBfRs for NO_3^- removal [14,20,24–26].

2.4. Analytical Methods of Aquatic Samples

Denitrification performance of the H_2 -based MBfR was ascertained by measuring the influent and effluent concentrations of NO_3^- and NO_2^- . The collected influent and effluent samples were filtered immediately through a 0.22 μm polyvinylidene fluoride (PVDF) syringe filter (Sangon Biotech, Shanghai, China), and then stored at 4 °C until analyzed. Aquatic NO_3^- and NO_2^- concentrations were analyzed by ion chromatography (ICS-1000, Dionex, Sunnyvale, CA, USA) equipped with a Dionex AS-19 column (4 × 250 mm, 4 μm) using 55 mM sodium hydroxide as the eluent. The NO_3^- concentrations inside the biofilm were determined by a microsensor measuring unit, and the detailed analytical procedure can be found in our previous research [27].

NO_3^- removal flux of the system (J in $\text{g}/(\text{m}^2\cdot\text{d})$) was calculated by Equation (1) [15,28].

$$J = \frac{Q}{A}(S_{\text{inf}} - S_{\text{eff}}) \quad (1)$$

where Q is the influent flow rate (m^3/d); A is the membrane surface area (m^2); and S_{inf} and S_{eff} are the influent and effluent NO_3^- concentrations (g/m^3), respectively.

2.5. Biofilm Sampling and Analysis

In order to evaluate the microbial community structure variation as a function of changing influent NO_3^- concentration, the biofilm sample was obtained by stripping off the entire biofilm from one of the 20 HFMs at the end of phases I, II, and III, named bio-sample N1, N2, and N3, respectively. Additionally, to figure out the microbial community structure at diverse locations of the biofilm fed with a specific NO_3^- loading, as shown in Figure 2, we sampled the biomass on a single HFM from the sampling ports 1, 2, and 3 (with a distance of 5, 20, and 35 cm from the H_2 supply end, respectively) at the end of phase III, which was named bio-sample D, M, and U, respectively. It should be noted that after the biofilm sampling at the end of phases I and II, new biofilms could be reconstructed on the single HFM within 14–21 days; meanwhile, stable NO_3^- removal was achieved at the remaining 19–26 days. All the bio-samples were stored at -80 °C until analyzed.

The collected bio-samples were delivered to Novogene Co., Ltd. (Suzhou, China) for high-throughput pyrosequencing analysis to investigate the structure and dynamics of the microbial community. Extraction of genomic DNA was conducted using the cetyltrimethylammonium bromide (CTAB)/sodium dodecyl sulfate (SDS) method [29], and bacterial 16S rRNA genes of V4-V5 regions were amplified using primers 515F (5'-GTGCCAGCMGCCGCGG-3') and 907R (5'-CCGTCAATTCMTTTRAGTTT-3') [30]. After purification with the Qiagen Gel Extraction Kit (Qiagen, Germany), the amplicon library was generated using the TruSeq DNA PCR-Free Kit (Illumina, San Diego, CA, USA). Paired-end reads were merged by using FLASH (V1.2.7), and high quality tags were screened on the basis of QIIME (V1.9.1) [31], then they were assigned into operational taxonomic units with a similarity threshold of 97% by Uparse V7.0.1001 [32]. The Silva Database [33] was

employed on the basis of the Mothur algorithm for taxonomic annotation, and sequence alignment was processed by the MUSCLE (V 3.8.31) [34]. PICRUSt, a classical and powerful platform for predicting functional genes [35,36], was applied based on the whole qualified sequencing results using the Kyoto Encyclopedia of Genes and Genomes (KEGG) database [37], and more details are provided in Langille et al. [38]. In this research, we especially focused on the KEEG orthology of nitrogen metabolism related pathways.

3. Results and Discussion

3.1. Denitrification Performance

After 60 days running of the H₂-based MBfR at conditions where HRT and NO₃⁻ loading equaled 10 h and 10 mg N/L, respectively, biofilms with a relatively uniform thickness of nearly 600 μm were naturally formed on the surface of the HFMs, and complete NO₃⁻ removal was achieved, implying the successful start-up of the system. Following the stabilization of the system after the HRT was shifted from 10 to 5 h, experiments were conducted to evaluate the effects of electron acceptor availability on the denitrification performance. As delineated in Figure 3, the effluent NO₃⁻ concentration in phases I, II, and III was 0.12, 0.77, and 7.86 mg N/L, respectively, and NO₂⁻ was only detected in the effluent in phase III with a concentration of 3.2 mg N/L. According to the existing reference [14], excessively high NO₃⁻ loading could lead to NO₂⁻ accumulation in the effluent of H₂-based MBfR. Noticeably, the average NO₃⁻ removal flux (calculated via Equation (1)) of the system was markedly enhanced from 0.67 g/(m²·d) to 1.31 g/(m²·d), as the influent NO₃⁻ concentration was increased from 10 mg N/L in phase I to 20 mg N/L in phase II, but the further increase of NO₃⁻ loading to 30 mg N/L in phase III merely resulted in a slightly higher NO₃⁻ removal efficiency (1.50 g/(m²·d)). In combination with the NO₃⁻ removal and NO₂⁻ accumulation results, it can be surmised that the relatively higher NO₃⁻ removal flux at the influent NO₃⁻ concentration of 30 mg N/L was because the quantity of the electron donor (H₂) was insufficient to completely reduce NO₂⁻ to N₂.

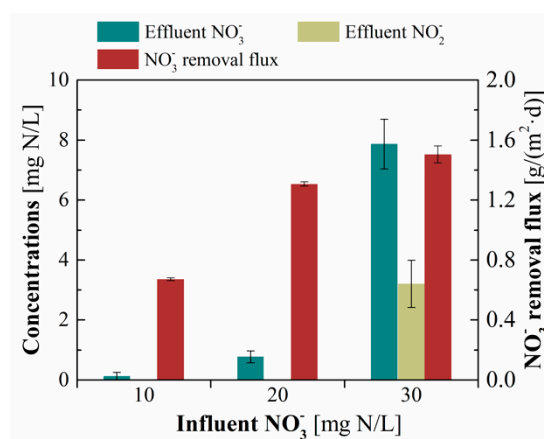


Figure 3. The effect of influent NO₃⁻ concentration on the denitrification performance of H₂-based MBfR.

The microsensor measurement results, as displayed in Figure 4, indicate that NO₃⁻ was always abundant at varying depths of the biofilm when 30 mg N/L NO₃⁻ was added to the influent, while an influent NO₃⁻ concentration of 20 mg N/L resulted in the formation of an inefficient denitrifying zone in the biofilm interior, where the DNB activity was inhibited because of the lower local NO₃⁻ concentration than the half-maximum-rate concentrations of NO₃⁻ for DNB ($K_{NO_3}^{DNB}$, 0.2 mg N/L) [39]. The above findings led us to reasonably extrapolate that the availability of electron donor (i.e., H₂) was the dominant limiting factor for NO₃⁻ removal in phase III. As illustrated earlier, the H₂ availability for biofilm utilization is directly subject to the back-diffusion of N₂ from the biofilm interior and bulk liquid. However, no single study exists that adequately covers the influence of the gases' back-diffusion on the dynamics of microbial communities in the counter-diffusional biofilm of a H₂-based MBfR.

Therefore, we concentrated in this study on the clarification of the microbial community structure characteristics of the counter-diffusional biofilm colonized on the close-end HFMs, which is conducive to furthering our comprehending of biofilm-related contaminant removal behavior.

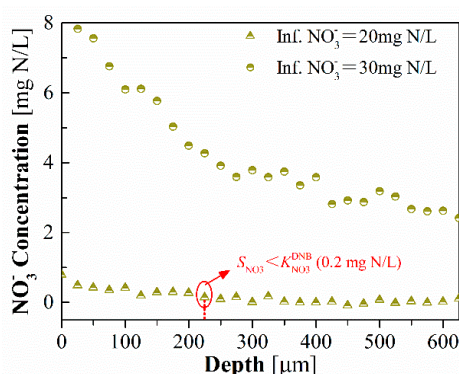


Figure 4. NO_3^- concentration gradients in biofilm at influent NO_3^- concentrations of 20 and 30 mg N/L. To the left of the plot is the bulk liquid side, while the right is the membrane side.

3.2. Microbial Community Analysis

To delve into the dynamics of microbial communities, the relatively high abundance of bacteria (top 8) at the genus level were investigated at different phases (bio-samples N1, N2, and N3) as well as distances from the H_2 supply end (bio-samples D, M, and U). The qualified sequence reads of bio-samples N1, N2, N3, D, M, and U were 59,290, 61,121, 65,304, 61,093, 62,610, and 47,935, respectively. As shown in Figure 5, in phase I, the most abundant genera pertaining to autotrophic denitrification process were found to be *Hydrogenophaga* and *Dechloromonas* with a relative abundance of 14.3% and 44.8%, respectively. *Hydrogenophaga*, known as an unculturable H_2 -oxidizing bacteria [40], played a dominant role in leading to NO_3^- removal in a number of H_2 -based MBfRs [41–43]. The genus of *Dechloromonas* was deemed to be capable of eliminating NO_3^- and ClO_4^- using dissimilatory nitrate reductases and/or specialized perchlorate reductases [42,44–46]. The further increase in influent NO_3^- concentration from 10 mg N/L in phase I to 20 mg N/L in phase II gave rise to the overwhelming percentage (relative abundance equals 49%) of *Hydrogenophaga* as well as the strikingly decreased population (<1.0%) of *Dechloromonas* in the biofilm. This is in accordance with the results of preceding studies that *Hydrogenophaga* outperformed *Dechloromonas* in terms of H_2 utilization and NO_3^- reduction in the case of an elevated NO_3^- loading [24,42,47]. Intriguingly, the relative abundance of *Hydrogenophaga* dropped to 17.2% at the influent NO_3^- concentration of 30 mg N/L in phase III. The possible explanations are the following: (1) the shortage of electron donors, which is supported by the observation that a mass of NO_3^- and NO_2^- was detected in the effluent, as exhibited in Figure 3; (2) the NO_2^- accumulation, given the susceptibility of *Hydrogenophaga* to toxicity of NO_2^- [1,13]; and (3) the enrichment of unidentified bacterial strains, which were affiliated to the order of *Sphingobacteriales*, and might be involved in the conversion process of NO_3^- to NO [48].

Concerning the microbial communities at diverse locations of the biofilm fed with influent containing 30 mg N/L NO_3^- , *Hydrogenophaga*, was always the primary genus regardless of the distance from the H_2 supply end, where its relative abundance was dramatically increased from 13.1% at the distance of 5 cm to 21.7% at the distance of 35 cm. This is unsurprising in light of the fact that attributed to the impact of back-diffusion, the quantity of H_2 that could penetrate the HFMs and be available for the utilization of DNB proliferated at different positions of biofilm was negatively correlated with the distance from the H_2 supply end. As a frequently discovered autotrophic DNB in H_2 -based MBfRs [19,47], *Methyloversatilis* was found to be the second most abundant functional bacteria for NO_3^- removal, possessing a relatively stable relative abundance ranging from 4.0–5.2% at varying locations of the biofilm. The unidentified *Sphingobacteriales*, a possible NO_3^- consumer as mentioned earlier, with its content variation tendency with changing positions was similar to that of *Hydrogenophaga*, but merely

occupied a quite lower population (0.3–1.4%). The unidentified_*Nitrospiraceae*, the well-known autotrophic nitrite-oxidizing bacteria (NOB) [43], preferred to enrich at the upper side instead of the lower side of the biofilm, presumably due to the fact that the low H_2 pressure at the upper side of the intramembrane facilitated the entrance into the biofilm and the subsequent consumption of trace of dissolved oxygen arisen from the influent by the NOB.

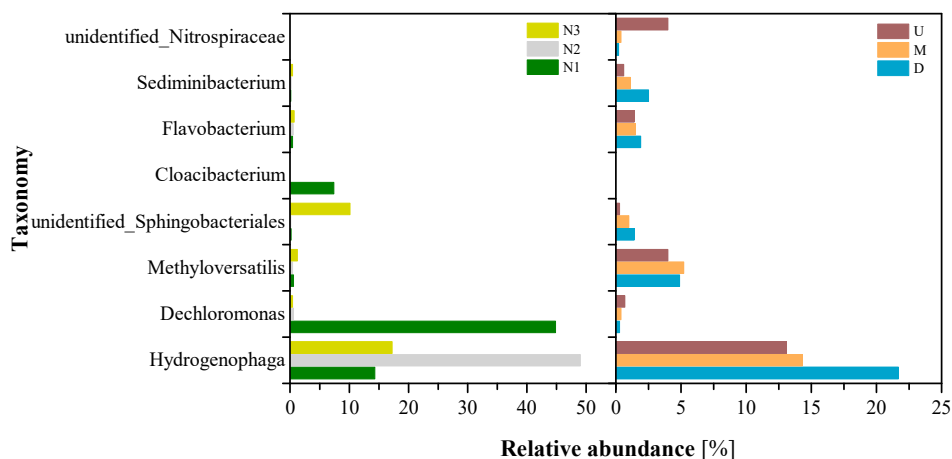


Figure 5. Taxonomic diversity of pyrosequences from bacterial communities at the genus level.

Throughout the whole experiment, other DNBs such as *Azonexus* [42,49] were detected in the bio-samples but with an exceedingly low relative abundance. Since SO_4^{2-} was included in the influent, some genera involved in sulfur reduction (*Desulfovibrio*, *Sediminibacterium*) [50,51] and sulfide oxidation (*Flavobacterium* and *Sulfuritalea*) [18,52] were also discovered, thus a sulfur-relating microcirculation could occur in the counter-diffusional biofilm.

3.3. Predictive Functional Genes

PICRUSt was applied to predict the functional genes in the bio-samples on the basis of the high-throughput sequencing results of the 16S rRNA gene, and the odds ratios of the predictive functional genes are summarized in Figure 6. The variation tendencies in predicted relative abundance of a few basic metabolic pathways including xenobiotics biodegradation and metabolism, membrane transport, and energy metabolism are in full agreement with those of the detected dominant DNB (i.e., *Hydrogenophaga*) at conditions of varying NO_3^- loadings and distances from the H_2 supply end. Xenobiotics biodegradation and metabolism is closely related to the resistance of microorganisms to the toxicity of the exogenous contaminant [53]. The predicted highest abundance (5.87%) of the genes relating to xenobiotics biodegradation and metabolism appeared in phase II, probably due to the largest population of *Hydrogenophaga* and poor accumulation of noxious intermediates at this stage. With a similar trend, membrane transport, known to play a fundamental role in the substantial and ATP transportation process [54], occupied a conspicuously greater relative abundance of 17.69% in phase II than those (9.11–14.47%) in phases I and III. The evolution of denitrification behavior of functional bacteria is correlated to the changes of the nitrogen metabolism-related genes, belonging to energy metabolism-related genes. The nitrogen metabolism-related genes were most abundant with a proportion of 0.95% in phase II. It is noteworthy that the gene abundance involved in nitrogen metabolism was increased from 0.83% in the upside to 0.88% in the downside of the biofilm; this mirrored the variation tendency in the abundance of the genes involved in membrane transport with changing distance from the H_2 supply end. The foregoing function prediction results can support that the microbial metabolism at different locations of the biofilm in the H_2 -based MBfR was significantly affected by the back-diffusion of inactive gases.

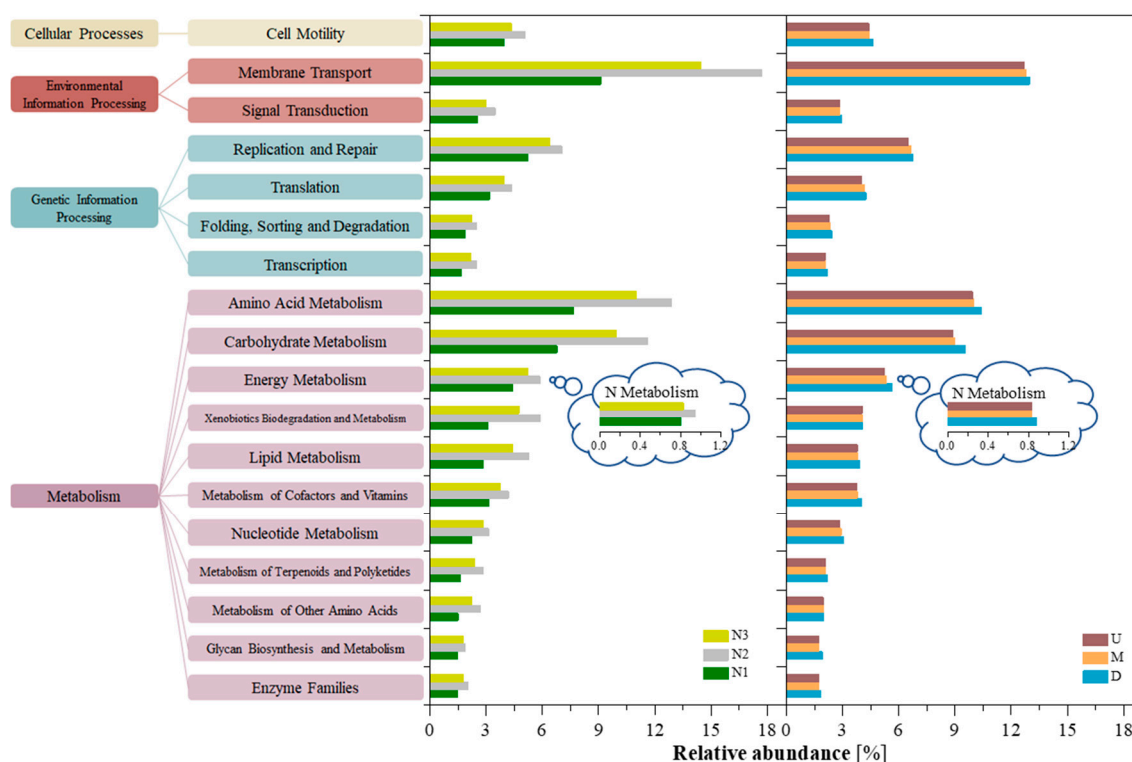
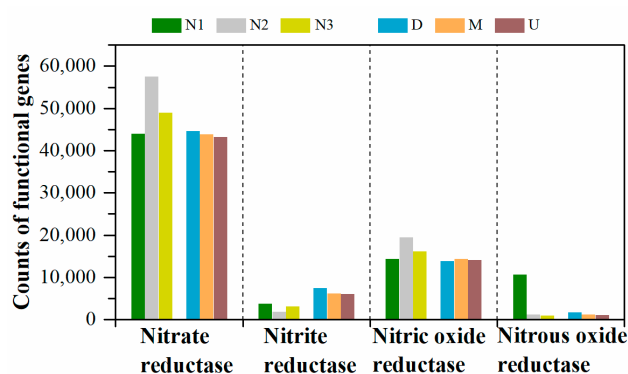


Figure 6. Odds ratios of predictive functional genes in the biofilm samples based on PICRUSt analysis. Genes with unknown functions and low relative abundance (<1%) are eliminated.

To figure out the nitrogen reductase involved in the nitrogen metabolism pathway, copy numbers of functional enzymes relating to the autotrophic denitrification process including nitrate, nitrite, nitric oxide, and nitrous oxide reductases were examined, as exhibited in Figure 7. The results regarding the counts of predictive functional genes encoding for nitrate reductase consisting of alpha subunit, beta subunit, gamma subunit, cytochrome, and electron transfer subunit are shown in Table 1. As to the influent NO_3^- concentration series, the largest counts of nitrate reductase genes of 57,554 and nitric oxide reductase genes of 19,475 were found in phase II, probably due to the greatest population of *Hydrogenophaga* genera in the biofilm, as shown in Figure 5. It is worth noting that despite the proportion of *Hydrogenophaga* and counts of nitrate enzyme genes in phase II were obviously greater than those in phase III (Figures 5 and 7), however, the NO_3^- removal flux in phase II was slightly lower than that in phase III (Figure 3). This can be ascribed to the decreased availability of NO_3^- for DNB in the biofilm interior in phase II (Figure 4), which gave rise to the declined overall activity of these functional bacteria. Although the nitrite reductase genes were more enriched in phase III rather than phase II, a considerable amount of NO_2^- was accumulated in the effluent in phase III (Figure 3). According to a preceding reference [27], the biofilm depth (from the bulk liquid side) that the electron donor (H_2) could reach was negatively correlated with NO_3^- loading; thus the activity of the nitrite reductase in DNB that grew in the vicinity of the HFM side might suffer from the shortage of H_2 . Regarding the nitrous oxide reductase genes, the counts in phase I were found to be strikingly greater than those in phases II and III. The limited expression of nitrous oxide reductase in phases II and III is presumably associated with the insufficient supply of electron donors in the case of high electron acceptor (NO_3^-) loading.

Table 1. Counts of predictive functional genes and descriptions involved in the nitrogen metabolism pathway.

Reductase	KO_Hierarchy	KEGG_Description	N1	N2	N3	D	M	U
Nitrate reductase	K00370	nitrate reductase alpha subunit	12,718	18,940	16,095	15,010	14,465	14,245
	K00371	nitrate reductase beta subunit	12,783	18,984	16,111	15,421	14,485	14,296
	K00374	nitrate reductase gamma subunit	8040	18,639	15,925	12,799	14,172	13,816
	K02567	nitrate reductase (cytochrome)	5236	501	437	694	372	408
	K02568	nitrate reductase (cytochrome), electron transfer subunit	5215	490	423	668	362	399
Nitrite reductase	K00368	nitrite reductase (NO-forming)	3676	1837	3077	7378	6180	6000
Nitric oxide reductase	K04561	nitric oxide reductase subunit B	14,325	19,475	16,173	13,828	14,392	14,122
Nitrous oxide reductase	K00376	nitrous-oxide reductase	10,580	1231	890	1666	1152	1040

**Figure 7.** Counts of predictive functional genes involved in the nitrogen metabolism pathway.

As the distance from the H_2 supply end was increased, the counts of nitrate, nitrite, and nitrous oxide reductase genes gradually decreased, with this variation trend identical to those in relative abundances of *Hydrogenophaga* and predicted genes involved in N metabolism. For instance, the counts of nitrate, nitrite, and nitrous oxide reductase genes in the biomass at the upside of HFMs was decreased by 1428, 1378, and 626, respectively, in comparison to those at the downside. This result offers evidence that the expression of most denitrifying enzymes of DNB in the biofilm was significantly hampered by the back-diffusion of inactive gases, especially those that grew at the locations far from the H_2 supply end. In particular, in most cases of diverse NO_3^- loading and distance from the H_2 supply end, the counts of genes encoding for nitrous oxide reductase are the fewest among denitrifying enzymes, likely as a consequence of the prioritized consumption of electron donor by other N metabolism-related enzymes in the case of electron donor deficiency. The relatively less expression of nitrous oxide reductase implies the possible accumulation of denitrifying intermediates (i.e., N_2O). A previous mechanism study results suggested that biofilm systems could result in obviously greater amount of N_2O emissions than suspended-growth systems, attributed to their nature in terms of microbial stratification and substrate gradients [55].

4. Conclusions

In this study, the NO_3^- removal performance and characteristics of microbial community structure were investigated in a close-end operated H_2 -based MBfR. Based on the analysis of the concentration variations of NO_3^- and/or its intermediate product (i.e., NO_2^-) in the effluent and biofilm as a function as changing NO_3^- loading, the H_2 availability for biofilm utilization was found to be the main limiting factor for NO_3^- removal at an influent NO_3^- concentration of 30 mg N/L. Microbial community analysis results suggest that at NO_3^- loadings of 20–30 mg N/L, *Hydrogenophaga* was always recognized as the dominant functional bacteria in the collected bio-samples, regardless of the distance from the H_2 supply end; an influent NO_3^- concentration of 20 mg N/L was found to facilitate the enrichment of *Hydrogenophaga*; the relative abundance of *Hydrogenophaga* was negatively correlated with the distance from the H_2 supply end. Functional genes analysis results corroborate that the variation trends of

relative abundance of basic metabolic pathways and counts of functional enzyme genes with varying NO_3^- loading and distance from the H_2 supply end are, in most cases, in good agreement with the population evolution of *Hydrogenophaga*; due to the impact of the gases' back-diffusion, a majority of functional genes pertaining to the microbial metabolism as well as the denitrification process gradually decreased from the downside to upside of HFMs.

Author Contributions: Conceptualization, H.L. (Haixiang Li) and X.Z.; Data curation, M.J., Y.Y. and Y.C.; Funding acquisition, J.Z. and H.L. (Haixiang Li); Investigation, M.J., Y.Y. and Y.C.; Methodology, M.J., Y.Y. and Y.C.; Project administration, J.Z. and H.L. (Haixiang Li); Resources, H.L. (Haixiang Li); Supervision, H.L. (Hua Lin); Visualization, M.J. and Y.Z.; Writing—original draft, M.J. and Y.Z.; Writing—review & editing, J.Z. All authors have read and agreed to the published version of the manuscript.

Funding: This research was funded by the Basic Ability Enhancement Program for Young and Middle-aged Teachers of Guangxi (grant number 2020KY05039); the National Natural Science Foundation of China (grant number 51878197); the Innovation Project of Guangxi Graduate Education (grant number YCBZ2017053); and Guangxi Collaborative Innovation Center for Water Pollution Control and Water Safety in Karst Area.

Conflicts of Interest: The authors declare no conflict of interest.

References

1. Wu, J.; Yin, Y.; Wang, J. Hydrogen-based membrane biofilm reactors for nitrate removal from water and wastewater. *Int. J. Hydrogen Energ.* **2018**, *43*, 1–15. [[CrossRef](#)]
2. Terada, A.; Hibiya, K.; Nagai, J.; Tsuneda, S.; Hirata, A. Nitrogen removal characteristics and biofilm analysis of a membrane-aerated biofilm reactor applicable to high-strength nitrogenous wastewater treatment. *J. Biosci. Bioeng.* **2003**, *95*, 170–178. [[CrossRef](#)]
3. Chen, M.; Price, R.M.; Yamashita, Y.; Jaffé, R. Comparative study of dissolved organic matter from groundwater and surface water in the Florida coastal Everglades using multi-dimensional spectrofluorometry combined with multivariate statistics. *Appl. Geochem.* **2010**, *25*, 872–880. [[CrossRef](#)]
4. Shen, Y.; Chapelle, F.H.; Strom, E.W.; Benner, R. Origins and bioavailability of dissolved organic matter in groundwater. *Biogeochemistry* **2015**, *122*, 61–78. [[CrossRef](#)]
5. Martin, K.J.; Nerenberg, R. The membrane biofilm reactor (MBfR) for water and wastewater treatment: Principles, applications, and recent developments. *Bioresour. Technol.* **2012**, *122*, 83–94. [[CrossRef](#)]
6. Terada, A.; Kaku, S.; Matsumoto, S.; Tsuneda, S. Rapid autohydrogenotrophic denitrification by a membrane biofilm reactor equipped with a fibrous support around a gas-permeable membrane. *Biochem. Eng. J.* **2006**, *31*, 84–91. [[CrossRef](#)]
7. Lee, K.C.; Rittmann, B.E. A novel hollow-fibre membrane biofilm reactor for autohydrogenotrophic denitrification of drinking water. *Water Sci. Technol.* **2000**, *41*, 219–226. [[CrossRef](#)]
8. Tang, Y.; Zhou, C.; Van Ginkel, S.W.; Ontiveros-Valencia, A.; Shin, J.; Rittmann, B.E. Hydrogen permeability of the hollow fibers used in H_2 -based membrane biofilm reactors. *J. Membr. Sci.* **2012**, *407–408*, 176–183. [[CrossRef](#)]
9. Xia, S.; Wang, C.; Xu, X.; Tang, Y.; Wang, Z.; Gu, Z.; Zhou, Y. Bioreduction of nitrate in a hydrogen-based membrane biofilm reactor using CO_2 for pH control and as carbon source. *Chem. Eng. J.* **2015**, *276*, 59–64. [[CrossRef](#)]
10. Healy, R.W.; Bartos, T.T.; Rice, C.A.; McKinley, M.P.; Smith, B.D. Groundwater chemistry near an impoundment for produced water, Powder River Basin, Wyoming, USA. *J. Hydrol.* **2011**, *403*, 37–48. [[CrossRef](#)]
11. Zhu, G.F.; Li, Z.Z.; Su, Y.H.; Ma, J.Z.; Zhang, Y.Y. Hydrogeochemical and isotope evidence of groundwater evolution and recharge in Minqin Basin, Northwest China. *J. Hydrol.* **2007**, *333*, 239–251. [[CrossRef](#)]
12. Perez-Calleja, P.; Aybar, M.; Picioreanu, C.; Esteban-Garcia, A.L.; Martin, K.J.; Nerenberg, R. Periodic venting of MABR lumen allows high removal rates and high gas-transfer efficiencies. *Water Res.* **2017**, *121*, 349–360. [[CrossRef](#)] [[PubMed](#)]
13. Xia, S.; Zhong, F.; Zhang, Y.; Li, H.; Yang, X. Bio-reduction of nitrate from groundwater using a hydrogen-based membrane biofilm reactor. *J. Environ. Sci.* **2010**, *22*, 257–262. [[CrossRef](#)]
14. Lee, K.-C.; Rittmann, B.E. Applying a novel autohydrogenotrophic hollow-fiber membrane biofilm reactor for denitrification of drinking water. *Water Res.* **2002**, *36*, 2040–2052. [[CrossRef](#)]

15. Zhao, H.-P.; Ontiveros-Valencia, A.; Tang, Y.; Kim, B.-O.; VanGinkel, S.; Friese, D.; Overstreet, R.; Smith, J.; Evans, P.; Krajmalnik-Brown, R.; et al. Removal of multiple electron acceptors by pilot-scale, two-stage membrane biofilm reactors. *Water Res.* **2014**, *54*, 115–122. [[CrossRef](#)]
16. Ahmed, T.; Semmens, M.J. The use of independently sealed microporous hollow fiber membranes for oxygenation of water: Model development. *J. Membr. Sci.* **1992**, *69*, 11–20. [[CrossRef](#)]
17. Li, H.; Zhou, L.; Lin, H.; Xu, X.; Jia, R.; Xia, S. Dynamic response of biofilm microbial ecology to para-chloronitrobenzene biodegradation in a hydrogen-based, denitrifying and sulfate-reducing membrane biofilm reactor. *Sci. Total Environ.* **2018**, *643*, 842–849. [[CrossRef](#)]
18. Long, M.; Ilhan, Z.E.; Xia, S.; Zhou, C.; Rittmann, B.E. Complete dechlorination and mineralization of pentachlorophenol (PCP) in a hydrogen-based membrane biofilm reactor (MBfR). *Water Res.* **2018**, *144*, 134–144. [[CrossRef](#)]
19. Li, H.; Zhou, L.; Lin, H.; Zhang, W.; Xia, S. Nitrate effects on perchlorate reduction in a H₂/CO₂-based biofilm. *Sci. Total Environ.* **2019**, *694*, 133564. [[CrossRef](#)]
20. Xia, S.; Liang, J.; Xu, X.; Shen, S. Simultaneous removal of selected oxidized contaminants in groundwater using a continuously stirred hydrogen-based membrane biofilm reactor. *J. Environ. Eng.* **2013**, *25*, 96–104. [[CrossRef](#)]
21. Su, X.; Wang, H.; Zhang, Y. Health risk assessment of nitrate contamination in groundwater: A case study of an agricultural area in Northeast China. *Water Resour. Manag.* **2013**, *27*, 3025–3034. [[CrossRef](#)]
22. Gu, B.; Ying, G.; Chang, S.X.; Luo, W.; Jie, C. Nitrate in groundwater of China: Sources and driving forces. *Glob. Environ. Chang.* **2013**, *23*, 1112–1121. [[CrossRef](#)]
23. Gao, S.; Li, C.; Jia, C.; Zhang, H.; Guan, Q.; Wu, X.; Wang, J.; Lv, M. Health risk assessment of groundwater nitrate contamination: A case study of a typical karst hydrogeological unit in East China. *Environ. Sci. Pollut. R.* **2020**, *27*, 9274–9287. [[CrossRef](#)] [[PubMed](#)]
24. Zhou, L.; Xu, X.; Xia, S. Effects of sulfate on simultaneous nitrate and selenate removal in a hydrogen-based membrane biofilm reactor for groundwater treatment: Performance and biofilm microbial ecology. *Chemosphere* **2018**, *211*, 254–260. [[CrossRef](#)] [[PubMed](#)]
25. Xia, S.; Xu, X.; Zhou, C.; Wang, C.; Zhou, L.; Rittmann, B.E. Direct delivery of CO₂ into a hydrogen-based membrane biofilm reactor and model development. *Chem. Eng. J.* **2016**, *290*, 154–160. [[CrossRef](#)]
26. Ontiveros-Valencia, A.; Ziv-El, M.; Zhao, H.-P.; Feng, L.; Rittmann, B.E.; Krajmalnik-Brown, R. Interactions between nitrate-reducing and sulfate-reducing bacteria coexisting in a hydrogen-fed biofilm. *Environ. Sci. Technol.* **2012**, *46*, 11289–11298. [[CrossRef](#)]
27. Jiang, M.; Zheng, J.; Perez-Calleja, P.; Picioreanu, C.; Lin, H.; Zhang, X.; Zhang, Y.; Li, H.; Nerenberg, R. New insight into CO₂-mediated denitrification process in H₂-based membrane biofilm reactor: An experimental and modeling study. *Water Res.* **2020**, *184*, 116177. [[CrossRef](#)]
28. Lai, C.-Y.; Yang, X.; Tang, Y.; Rittmann, B.E.; Zhao, H.-P. Nitrate Shaped the Selenate-Reducing Microbial Community in a Hydrogen-Based Biofilm Reactor. *Environ. Sci. Technol.* **2014**, *48*, 3395–3402. [[CrossRef](#)]
29. Ding, X.W.; Wei, D.; Guo, W.S.; Wang, B.; Meng, Z.J.; Feng, R.; Du, B.; Wei, Q. Biological denitrification in an anoxic sequencing batch biofilm reactor: Performance evaluation, nitrous oxide emission and microbial community. *Bioresour. Technol.* **2019**, *285*, 9. [[CrossRef](#)]
30. Lai, C.-Y.; Wen, L.-L.; Zhang, Y.; Luo, S.-S.; Wang, Q.-Y.; Luo, Y.-H.; Chen, R.; Yang, X.; Rittmann, B.E.; Zhao, H.-P. Autotrophic antimonate bio-reduction using hydrogen as the electron donor. *Water Res.* **2016**, *88*, 467–474. [[CrossRef](#)]
31. Caporaso, J.G.; Kuczynski, J.; Stombaugh, J.; Bittinger, K.; Bushman, F.D.; Costello, E.K.; Fierer, N.; Peña, A.G.; Goodrich, J.K.; Gordon, J.I.; et al. QIIME allows analysis of high-throughput community sequencing data. *Nat. Methods* **2010**, *7*, 335–336. [[CrossRef](#)] [[PubMed](#)]
32. Haas, B.J.; Gevers, D.; Earl, A.M.; Feldgarden, M.; Ward, D.V.; Giannoukos, G.; Ciulla, D.; Tabbaa, D.; Highlander, S.K.; Sodergren, E.; et al. Chimeric 16S rRNA sequence formation and detection in Sanger and 454-pyrosequenced PCR amplicons. *Genome Res.* **2011**, *21*, 494–504. [[CrossRef](#)] [[PubMed](#)]
33. Quast, C.; Pruesse, E.; Yilmaz, P.; Gerken, J.; Schweer, T.; Yarza, P.; Peplies, J.; Glöckner, F.O. The SILVA ribosomal RNA gene database project: Improved data processing and web-based tools. *Nucleic Acids Res.* **2013**, *41*, D590–D596. [[CrossRef](#)] [[PubMed](#)]
34. Edgar, R.C. MUSCLE: Multiple sequence alignment with high accuracy and high throughput. *Nucleic Acids Res.* **2004**, *32*, 1792–1797. [[CrossRef](#)]

35. Long, M.; Zeng, C.; Wang, Z.; Xia, S.; Zhou, C. Complete dechlorination and mineralization of para-chlorophenol (4-CP) in a hydrogen-based membrane biofilm reactor (MBfR). *J. Clean. Prod.* **2020**, *276*, 123257. [[CrossRef](#)]
36. Lv, P.L.; Shi, L.D.; Dong, Q.Y.; Rittmann, B.; Zhao, H.P. How nitrate affects perchlorate reduction in a methane-based biofilm batch reactor. *Water Res.* **2020**, *171*, 115397. [[CrossRef](#)]
37. Pang, Y.; Wang, J. Insight into the mechanism of chemoautotrophic denitrification using pyrite (FeS₂) as electron donor. *Bioresour. Technol.* **2020**, *318*, 124105. [[CrossRef](#)]
38. Langille, M.G.I.; Zaneveld, J.; Caporaso, J.G.; McDonald, D.; Knights, D.; Reyes, J.A.; Clemente, J.C.; Burkepile, D.E.; Thurber, R.L.V.; Knight, R.; et al. Predictive functional profiling of microbial communities using 16S rRNA marker gene sequences. *Nat. Biotechnol.* **2013**, *31*, 814–821. [[CrossRef](#)]
39. Tang, Y.; Zhao, H.; Marcus, A.K.; Krajmalnik-Brown, R.; Rittmann, B.E. A steady-state biofilm model for simultaneous reduction of nitrate and perchlorate, part 1: Model development and numerical solution. *Environ. Sci. Technol.* **2012**, *46*, 1598–1607. [[CrossRef](#)]
40. Park, H.I.; Choi, Y.-J.; Pak, D. Autohydrogenotrophic Denitrifying microbial community in a glass beads biofilm reactor. *Biotechnol. Lett.* **2005**, *27*, 949–953. [[CrossRef](#)]
41. Zhang, Y.; Zhong, F.; Xia, S.; Wang, X.; Li, J. Autohydrogenotrophic denitrification of drinking water using a polyvinyl chloride hollow fiber membrane biofilm reactor. *J. Hazard. Mater.* **2009**, *170*, 203–209. [[CrossRef](#)] [[PubMed](#)]
42. Zhao, H.-P.; Van Ginkel, S.; Tang, Y.; Kang, D.-W.; Rittmann, B.; Krajmalnik-Brown, R. Interactions between Perchlorate and Nitrate Reductions in the Biofilm of a Hydrogen-Based Membrane Biofilm Reactor. *Environ. Sci. Technol.* **2011**, *45*, 10155–10162. [[CrossRef](#)] [[PubMed](#)]
43. Park, J.-H.; Choi, O.; Lee, T.-H.; Kim, H.; Sang, B.-I. Pyrosequencing analysis of microbial communities in hollow fiber-membrane biofilm reactors system for treating high-strength nitrogen wastewater. *Chemosphere* **2016**, *163*, 192–201. [[CrossRef](#)] [[PubMed](#)]
44. Ontiveros-Valencia, A.; Tang, Y.; Krajmalnik-Brown, R.; Rittmann, B.E. Perchlorate reduction from a highly contaminated groundwater in the presence of sulfate-reducing bacteria in a hydrogen-fed biofilm. *Biotechnol. Bioeng.* **2013**, *110*, 3139–3147. [[CrossRef](#)] [[PubMed](#)]
45. Xia, S.; Wu, C.; Yang, X.; Zhou, Y.; Zhou, L.; Ran, Y.; Rittmann, B.E. Bioreduction of nitrate in high-sulfate water using a hydrogen-based membrane biofilm reactor equipped with a separate carbon dioxide module. *Chem. Eng. J.* **2020**, *385*, 123831. [[CrossRef](#)]
46. Zhao, H.P.; Ontiveros-Valencia, A.; Tang, Y.N.; Kim, B.O.; Ilhan, Z.E.; Krajmalnik-Brown, R.; Rittmann, B. Using a two-stage hydrogen-based membrane biofilm reactor (MBfR) to achieve complete perchlorate reduction in the presence of nitrate and sulfate. *Environ. Sci. Technol.* **2013**, *47*, 1565–1572. [[CrossRef](#)]
47. Ontiveros-Valencia, A.; Ilhan, Z.E.; Kang, D.-W.; Rittmann, B.; Krajmalnik-Brown, R. Phylogenetic analysis of nitrate- and sulfate-reducing bacteria in a hydrogen-fed biofilm. *FEMS Microbiol. Ecol.* **2013**, *85*, 158–167. [[CrossRef](#)]
48. Wei, Z.S.; Wang, J.B.; Huang, Z.S.; Xiao, X.L.; Tang, M.R.; Li, B.L.; Zhang, X. Removal of nitric oxide from biomass combustion by thermophilic nitrification-aerobic denitrification combined with catalysis in membrane biofilm reactor. *Biomass Bioenerg.* **2019**, *126*, 34–40. [[CrossRef](#)]
49. Quan, Z.-X.; Im, W.-T.; Lee, S.-T. *Azonexus caeni* sp. nov., a denitrifying bacterium isolated from sludge of a wastewater treatment plant. *Int. J. Syst. Evol. Micr.* **2006**, *56*, 1043–1046. [[CrossRef](#)]
50. Qu, J.-H.; Yuan, H.-L. *Sediminibacterium salmoneum* gen. nov., sp. nov., a member of the phylum Bacteroidetes isolated from sediment of a eutrophic reservoir. *Int. J. Syst. Evol. Micr.* **2008**, *58*, 2191–2194. [[CrossRef](#)]
51. Ontiveros-Valencia, A.; Tang, Y.; Krajmalnik-Brown, R.; Rittmann, B.E. Managing the interactions between sulfate-and perchlorate-reducing bacteria when using hydrogen-fed biofilms to treat a groundwater with a high perchlorate concentration. *Water Res.* **2014**, *55*, 215–224. [[CrossRef](#)] [[PubMed](#)]
52. Watanabe, T.; Kojima, H.; Fukui, M. Complete genomes of freshwater sulfur oxidizers *Sulfuricella denitrificans* skB26 and *Sulfuritalea hydrogenivorans* sk43H: Genetic insights into the sulfur oxidation pathway of betaproteobacteria. *Syst. Appl. Microbiol.* **2014**, *37*, 387–395. [[CrossRef](#)] [[PubMed](#)]
53. Fetzner, S. Biodegradation of Xenobiotics. In *Biotechnology; Encyclopedia of Life Support Systems (EOLSS)*; EOLSS Publishers Co., Ltd.: Oxford, UK, 2002; pp. 215–246.

54. Rice, A.J.; Park, A.; Pinkett, H.W. Diversity in ABC transporters: Type I, II and III importers. *Crit. Rev. Biochem. Mol.* **2014**, *49*, 426–437. [[CrossRef](#)] [[PubMed](#)]
55. Sabba, F.; Piciooreanu, C.; Boltz, J.P.; Nerenberg, R. Predicting N₂O emissions from nitrifying and denitrifying biofilms: A modeling study. *Water Sci. Technol.* **2017**, *75*, 530–538. [[CrossRef](#)] [[PubMed](#)]

Publisher's Note: MDPI stays neutral with regard to jurisdictional claims in published maps and institutional affiliations.



© 2020 by the authors. Licensee MDPI, Basel, Switzerland. This article is an open access article distributed under the terms and conditions of the Creative Commons Attribution (CC BY) license (<http://creativecommons.org/licenses/by/4.0/>).